ELSEVIER

Chemical Geology 194 (2003) 41–49

CHEMICAL GEOLOGY
INCLUDING
ISOTOPE GEOSCIENCE

www.elsevier.com/locate/chemgeo

Calibration of methane analysis by Raman spectroscopy in H_2O–NaCl–CH_4 fluid inclusions

Damien Guillaume*, Stéphane Teinturier, Jean Dubessy, Jacques Pironon

Equipe Interactions entre Fluides et Minéraux, UMR 7566 (G2R) et CREGU-(Entree 3B-5° etage), Géologie et Gestion des Ressources Minérales et Energétiques, Faculté des Sciences-Université Henri Poincaré, BP-239, 54506-Vandoeuvre-les Nancy Cedex, France

Received 28 November 2001; received in revised form 4 June 2002

Abstract

Calibration of the determination of CH_4/H_2O ratio using Raman spectroscopy is carried out using synthetic fluid inclusions at different NaCl concentration (0, 0.05, 0.66, 0.98, 1.00, 1.60, 2.25 and 3.5 m NaCl). Spectra of the stretching bands of methane and water in the aqueous phase were collected at variable temperatures up to a few degrees above the homogenisation temperature. The composition of the aqueous phase for temperatures below the homogenisation temperature was calculated with a computer program, using the model of Duan et al. [Geochim. Cosmochim. Acta 56 (1992) 1451]. Results show the dependency of the estimate of the CH_4 concentration on salinity: at constant CH_4 concentration, the CH_4/H_2O area ratio of Raman bands decreases with increasing salinity from 0 to 1.6 m and remains constant up to 3.5 m NaCl. The $P-T$ projection of the isopleth of a natural fluid inclusion is deduced from the homogenisation temperature, its composition obtained from cryometry (mNaCl eq.) and Raman analysis (mCH_4) ratio. This methodology was applied to a sample from the Cave-in-Rock MVT deposit (fluorite–Pb–Zn district, southern Illinois, USA) presenting petroleum fluid inclusions associated with fluid inclusions of the system H_2O–NaCl–CH_4. Hydrocarbon isochore intersects the isopleth of the H_2O–NaCl–CH_4 inclusions at the homogenization temperature, which validates this procedure.

Keywords: Fluid inclusions; H_2O–CH_4–NaCl system; Methane analysis; Raman spectroscopy; Petroleum fluid inclusions; Diagenetic fluids

1. Introduction

$P-T-t$ path reconstruction of a sedimentary basin is a key parameter for the evaluation of oil potential of sedimentary basins. Fluid inclusions that trap diagenetic fluids are a powerful tool for the reconstruction of $P-T$ conditions provided the composition is correctly determined. Natural crude oils are made of a mixture of hydrocarbons. The solubility of individual hydrocarbon components in water decreases rapidly with increasing molecular weight. Methane is the main hydrocarbon whose solubility in water is significant in the $P-T$ conditions of sedimentary basins (Price, 1981).

The methane concentration in formation waters in sedimentary basins is often low, below 0.3 m, and its quantification using microthermometric measure-

* Corresponding author. Tel.: +33-3-83-91-38-16; fax: +33-3-83-68-47-01.
E-mail addresses: damien.guillaume@g2r.uhp-nancy.fr (D. Guillaume), stephane.teinturier@g2r.uhp-nancy.fr (S. Teinturier), jean.dubessy@g2r.uhp-nancy.fr (J. Dubessy), jacques.pironon@g2r.uhp-nancy.fr (J. Pironon).

0009-2541/02/$ - see front matter © 2002 Published by Elsevier Science B.V.
PII: S0009-2541(02)00270-X

ments is not possible (Dubessy et al., 2001). However, neglecting small concentrations of methane may result in the incorrect interpretation of fluid inclusion observations because the pressure at the homogenisation temperature along the $L-V$ isopleth curve is underestimated (Fig. 1). Bulk concentration of methane in aqueous fluid inclusions can be obtained a few degrees above the homogenisation in the H_2O-CH_4 system (Dubessy et al., 2001). However, NaCl is always present in diagenetic fluids. In a $P-T$ diagram, the salting-out effect shifts the $L-V$ isopleth to a higher pressure (Fig. 1). Cl^- ion is a hydrogen bond breaker that strongly modifies the profile of the Raman band of the stretching vibration of water (Dubessy et al., in press), and prevents a priori of any extrapolation of the calibration of the H_2O-CH_4 ratio obtained from H_2O-CH_4 fluids. Therefore, the analysis of methane dissolved in $H_2O-NaCl$ fluid requires specific calibration as a function of the NaCl concentration. Such calibration is carried out using synthetic fluid inclusions prepared in fluorite and quartz crystals.

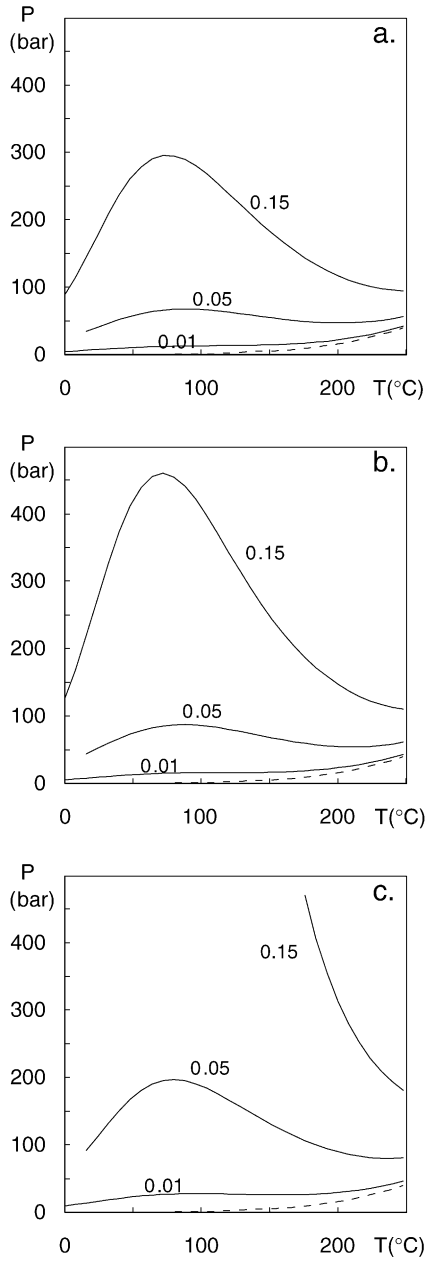

Fig. 1. Projection of the isopleth in the $P-T$ plane of the H_2O-CH_4-NaCl system calculated using the model of Duan et al. (1992). (a) 0 m NaCl; (b) 1 m NaCl; (c) 4 m NaCl. Labels refer to CH_4 concentration (molality scale), dashed lines: 0 m CH_4.

Petroleum fluids, which always contain significant amounts of methane, often more than 30 mol%, coexist with aqueous fluids during their migration in sedimentary basins. Methane being the most soluble hydrocarbon in aqueous phase, this gas component is expected to be present in the aqueous solutions at equilibrium with hydrocarbons. Therefore, $P-T$ conditions of trapping can be deduced from fluid inclusions representative of hydrocarbons and methane bearing aqueous solutions. This approach is applied to a sample from the Cave-in-Rock MVT deposit (fluorite–Pb–Zn district, southern Illinois, USA) with the PIT modelling of the $P-T$ projection of the bubble curve and isochore of the petroleum inclusions (Thiéry et al., 2000).

2. Experimental procedure

2.1. Starting materials

Synthetic fluid inclusions were produced in natural Brazilian quartz and synthetic fluorite (®SOREM). Water was taken from the distilled water supply of the laboratory (Millipore MILLI-Q® Reagent water system). CH_4 was supplied by Air Liquide® (99.9% minimum purity) and NaCl by Aldrich® (98% minimum purity).

Table 1
Experimental conditions of synthesis of fluid inclusions in the H_2O-CH_4-NaCl system and microthermometric data

Exp.	T_{exp} (°C)	P (bar)	mCH_4	Tm_{ice} (°C)	$Th_{L+V\rightarrow L}$ (°C)	mNaCl
1	200 ± 1	100 ± 5	0.102 ± 0.010	− 3.9 ± 0.1	200 ± 1	1.00 ± 0.03
2	201 ± 1	200 ± 5	0.195 ± 0.019	− 6.2 ± 0.1	201 ± 1	1.60 ± 0.03
3	200 ± 2	100 ± 5	0.083 ± 0.008	− 7.9 ± 0.1	201 ± 1	2.25 ± 0.03
4	200 ± 2	120 ± 5	0.074 ± 0.007	− 14.2 ± 0.1	201 ± 1	3.50 ± 0.03
5	150 ± 2	200 ± 5	0.130 ± 0.013	− 3.3 ± 0.1	150 ± 1	0.98 ± 0.03
6	250 − 200	205 ± 5	0.298 ± 0.030	− 2.2 ± 0.05	234 ± 1	0.66 ± 0.02
7	200 − 150	195 ± 5	0.210 ± 0.021	− 0.2 ± 0.05	186 ± 1	0.05 ± 0.02
8	198 ± 2	205 ± 5	0.240 ± 0.024	0.0 ± 0.05	197 ± 1	0.00 ± 0.02

Exp.: experiments. Experiments 1–4: fluorite experiments, Experiments 5–8: quartz experiments. P (bar): total pressure measured at experimental temperature T (°C); mCH_4: CH_4 molality calculated at Th (°C), for measured total pressure and NaCl concentration calculated using the model of Duan et al. (1992). Tm_{ice} (°C): ice melting temperature. $Th_{L+V\rightarrow L}$ (°C): homogenisation temperature to the liquid phase.

2.2. Formation of fluid inclusions

In quartz crystals, fluid inclusions were formed using preexisting inclusion cavities (20–40 μm) which were previously decrepitated. In fluorite crystals, cavities were made using the laser ablation method (Dubessy et al., 2000). All experiments were conducted in a gas-pressure autoclave. The major advantage of this autoclave is to maintain the equilibrium between liquid and vapour phase at run conditions. Crystal samples with preformed cavities were put inside the aqueous liquid phase of known salinity inside the autoclave. Oxygen and nitrogen gases of the air above the aqueous solution were flushed out by methane bubbling at room temperature before heating. Temperature and pressure were controlled during the experiments (Table 1). For runs 6 and 7, a gentle cooling was applied to enhance quartz cementation (5 °C/day during 10 days). In fluorite crystals, two types of fluid inclusions were produced: inclusions with cavities around 15 μm in diameter (Fig. 2a) and smaller inclusions in the sealed cracks around the cavities. Fig. 2b shows the typical morphology of inclusions obtained in quartz crystals. The methane concentration in the aqueous phase is calculated using the thermodynamic model of Duan et al. (1992).

2.3. Analytical techniques

Microthermometric measurements were obtained using a Chaix Meca heating and freezing stage (Poty et al., 1976). The Raman microprobe is a Labram type (®Dilor) with a ®Notch filter and with a CCD detector cooled at − 30 °C. The exciting radiation at 514.532 nm is provided by an Ar^+ laser (type 2020, ®Spectraphysics). A grating of 1800 grooves/mm is

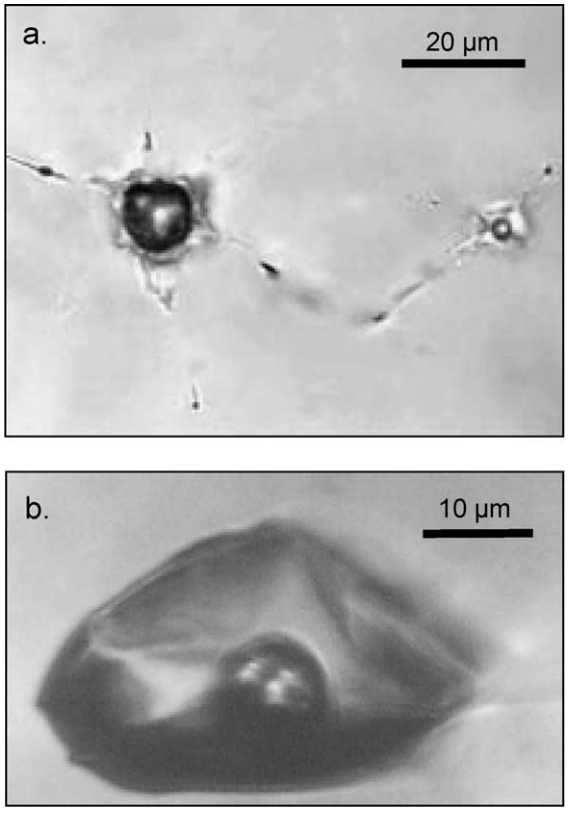

Fig. 2. (a) Photomicrograph of inclusions obtained in sealed cavities formed by laser ablation in fluorite crystal. (b) Photomicrograph of a fluid inclusion obtained using preexisting decrepitated inclusion in natural quartz crystal.

chosen to combine good spectral resolution (around 2 cm^{-1}) and convenient spectral window. The Raman spectra are collected between 2800 and 3900 cm^{-1} to get simultaneously the symmetric stretching vibration of methane at 2910 cm^{-1} and the broad band corresponding to the stretching vibrations of water. Raman data were obtained below and a few degrees above homogenisation temperature using a Chaix Meca or Linkam stage fixed on the microscope of the Raman microprobe.

3. Results

3.1. Calibration

Temperatures of ice-melting and bulk homogenisation to the liquid phase were measured (Table 1). NaCl concentration is determined from the ice-melting temperature of the inclusion and is in good agreement with the salt concentration of the initial aqueous solution introduced into the autoclave. Samples obtained at constant temperature display fluid inclusion homogenisation temperatures equal to the measured experimental temperatures within the experimental errors ($\pm$ 1 or 2 °C, runs 1–5 and 8, Table 1). This feature is in agreement with the trapping of a liquid phase coexisting with a vapour phase (Ramboz et al., 1982). Thus, the aqueous inclusions can be considered to be representative of the liquid aqueous phase at equilibrium with the methane-bearing vapour phase. This finding is also confirmed by other experiments. First, healing of fractures around the laser ablation cavities occurs after 1 week (Dubessy et al., 2000). Secondly, experiments of solubility of ethylbenzene in aqueous solutions (Sawamura et al., 1989; Guillaume et al., 2001) have shown that the time to reach equilibrium was less than 1 day. Finally, if equilibrium was not achieved, the homogenisation temperature should be smaller than the experimental temperature. Therefore, the validation of the equilibrium between the aqueous and vapour phases justifies the calculation of the bulk methane concentration with the model of Duan et al. (1992). For samples prepared during cooling experiments, equilibrium between vapour and liquid aqueous phases is assumed to have occurred at a temperature equal to the homogenisation temperature. At temperatures lower than the homogenisation temperature, the inclusion is in the two-phase field and the methane concentration in the liquid aqueous phase is calculated with the algorithm of Dubessy et al. (2001).

Raman spectra obtained for different temperatures and for a given salt concentration are plotted in Fig. 3. They show the increase of the band intensity assigned to the symmetric stretching vibration of methane (v_1) around 2910 cm^{-1}, indicating the progressive dissolution of methane in the aqueous solution. On the other hand, it has been observed that its wave number does not change with temperature and salt concentration, indicating that the perturbation endeavoured by the molecules of methane remains constant over this range of density, composition and temperature.

Plot of mCH_4 versus the Raman band area ratio [$I(CH_4)/I(H_2O)$] (Fig. 4) shows the following features:

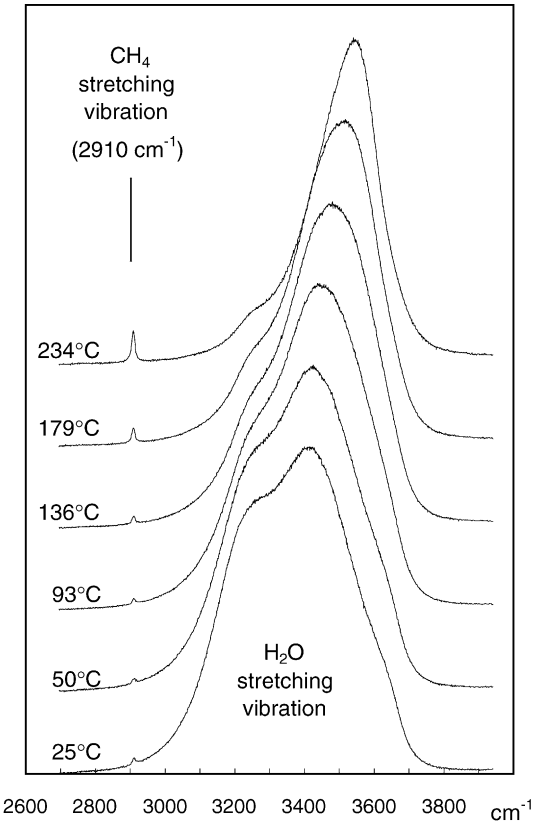

Fig. 3. Raman spectra obtained at several temperatures for a fluid inclusion in quartz having the following composition: NaCl, 0.66 m; CH_4, 0.298 m.

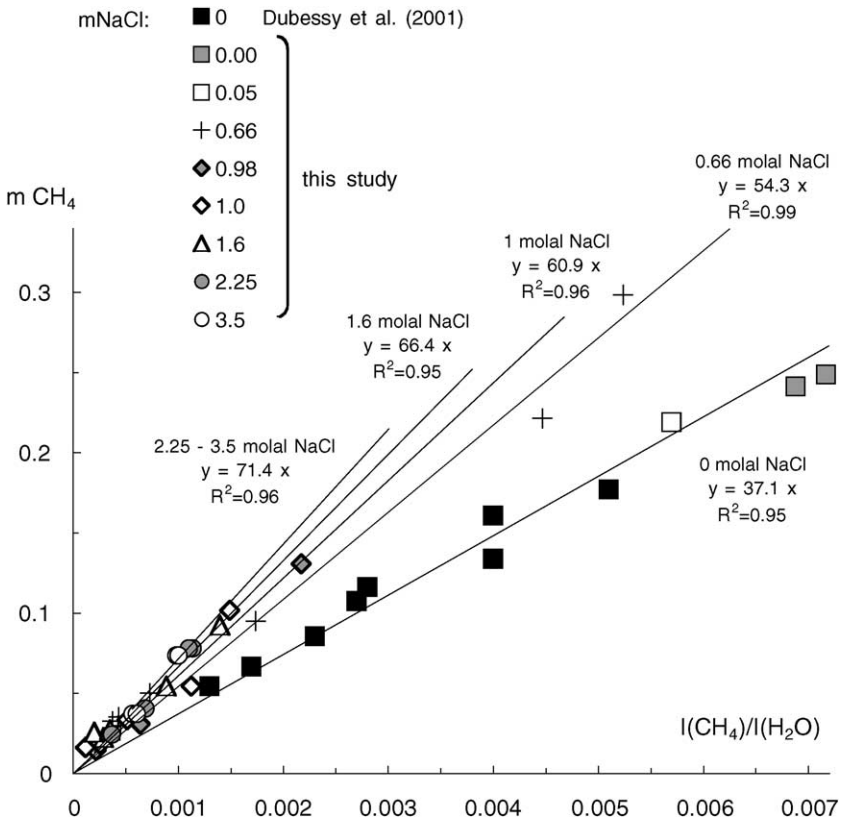

Fig. 4. Plot of the methane concentration (molality scale) versus the Raman band area ratio $I(CH_4)/I(H_2O)$. Labels indicate the salt concentration (molality scale), the regression line equation calculated from experimental data and the R^2 values of the fitted lines.

first, for a given salt concentration, data plot along a straight line although the temperatures are different along each line. The effect of temperature over the range of measurements (100–250 °C) is weak and does not modify the CH_4 molar estimate. Second, the different *iso*-salinity lines have a slope that depends on the salt concentration. A plot of this slope as a function of salinity is given in Fig. 5. For increasing salinity, the slope increases exponentially. The methane concentration (mCH_4) can be calculated with Eq. (1).

$$mCH_4 = [I(CH_4)/I(H_2O)] \times [72 - 35\ \exp(-1.1\ \mathrm{mNaCl})] \quad R^2 = 0.99 \tag{1}$$

where mNaCl is the salinity (molality scale) calculated from ice-melting temperature of the inclusion and $[I(CH_4)/I(H_2O)]$ is the Raman band area ratio.

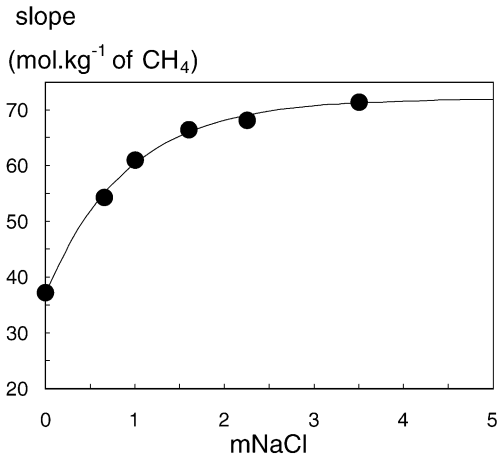

Fig. 5. Plot of the slope obtained by regression along data (Fig. 4) versus the corresponding NaCl concentration (molality scale).

The accuracy varies with the signal/background ratio. This ratio is dependent to the inclusion geometry and location to the surface of the sample. However, for the synthetic inclusions used for the calibration (up to 40 μm in size and 10–60 μm in depth), the accuracy determined from the R^2 value is around 10%. Eq. (1) integrates the apparatus function.

It is reasonable to expect that the Raman scattering cross-section of the symmetric stretching band of methane remains quasi constant at a fixed temperature and for different salinities and thus can be considered as an internal standard. These new data suggest that the Raman scattering cross-sections of OH oscillators increase with increasing NaCl concentration. The slope (Fig. 5) increases with increasing NaCl concentration, but this effect is weak above 1 m of NaCl and the absence of salinity effects above 1.6 m indicates that the structure of water is strongly modified between 0 and 1.6 m of NaCl concentration.

3.2. Effect of host mineral nature and orientation

Calibration curves that have been calculated between run 1 (200 °C, 1 m of NaCl, in isotropic fluorite crystal) and run 5 (150 °C, 0.98 m of NaCl, in birefringent quartz crystal) are consistent. This observation first confirms that there is no significant effect of host mineral nature. It also illustrates that temperature has no significant effect on mCH_4 estimate between 150 and 200 °C.

Spectra have been collected in the liquid phase of a single fluid inclusion (run 5) at 25 and 270 °C (above the homogenisation temperature) for various orientations of the crystal. Results are presented in Fig. 6. It appears that the orientation of birefringent mineral (quartz) has no significant effect on the calculated $I(CH_4)/I(H_2O)$ ratio and, as a consequence, no influence on the calculation of the methane concentration. Maximum deviation is below 5%.

3.3. Application to a case study

We studied inclusions trapped in fluorite from the Cave-in-Rock MVT deposit, fluorite–Pb–Zn district (Richardson and Pinckney, 1984; Roedder, 1984; Pironon et al., 1998). In a sample of fluorite, we studied a particular plane of fluid inclusions containing petroleum inclusions (5) together with

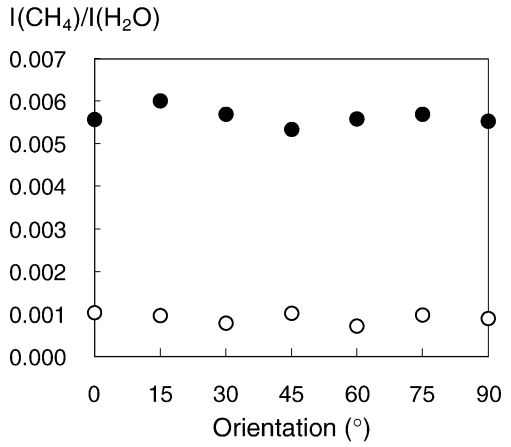

Fig. 6. $I(CH_4)/I(H_2O)$ ratio of a single fluid inclusion (run 5) for various orientation of birefringent host mineral (quartz). 0° = extinction. Spectra were collected in the liquid phase at 25 °C (open circles) and above homogenisation temperature (170 °C, filled circles). Maximum deviation is below 5%.

aqueous fluid inclusions (>20) (Fig. 7), this indicating that these palaeofluids were contemporaneous. Therefore, the petroleum and aqueous fluid inclusions are interpreted as the two immiscible fluids at equilibrium. The bulk homogenisation of fluid inclusions representative of the two end-members should be the same and representative of the temperature of trapping. The aqueous fluid inclusions of this particular plane homogenise at 145 ± 2 °C, whereas the petroleum inclusions homogenise at 112 ± 1 °C. Vapour filling of hydrocarbon inclusion, measured with confocal scanning laser microscope (Pironon et al., 1998), is 9 ± 0.5% at room temperature. The phase transition measured for petroleum inclusions is the homogenisation temperature of the petroleum phase and its significance deserves to be discussed. The solubility of water in petroleum is around 1 wt.% at 150 °C (Tsonopoulos and Wilson, 1983; Heidman et al., 1985; Sawamura et al., 1989; Guillaume et al., 2001). Such water concentration corresponds approximately to a coating of water with a thickness smaller than 0.1 μm, a value much smaller than the resolving power of the optical microscope. Consequently, the true homogenisation temperature of hydrocarbon fluid inclusions is expected to be higher than the temperature of partial homogenisation of the hydrocarbon part that can never be

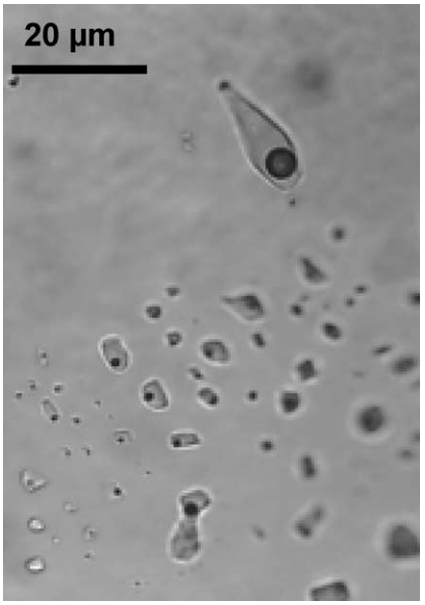

Fig. 7. Photomicrograph of petroleum and aqueous contemporaneous fluid inclusions in fluorite crystal from the Cave-in-Rock MVT deposit, fluorite–Pb–Zn district, southern Illinois, USA.

interpreted as the trapping temperature (Pironon et al., 2000). Therefore, a good approximation of the $P-T$ conditions of trapping is the intersection of the petroleum inclusion isochore with the isopleth of the methane bearing aqueous inclusion.

Eutectic temperatures of aqueous inclusions near -27 °C confirm that sodium is the dominant cation. The salinity, determined by ice-melting temperature, is 4 m equivalent NaCl. The $P-T$ projection of the possible bubble curves of the hydrocarbon part of the inclusion was calculated with the PIT software program (Thiéry et al. 2000) for a hydrocarbon homogenisation temperature of 112 ± 1 °C and a vapour volume fraction of 0.09 ± 0.005 (Fig. 8). The homogenisation pressure is 98 bars and the isochores correspond to the possible $P-T$ couples of data for trapping conditions. For coexisting petroleum and aqueous inclusions, the trapping conditions should be located at $T = 145 \pm 2$ °C (aqueous inclusions Th) and then at a pressure of $P = 230 \pm 15$ bar. For such $P-T$ conditions and NaCl concentration of 4 m in aqueous inclusions, the methane concentration at saturation calculated from the model of Duan et al. (1992) is

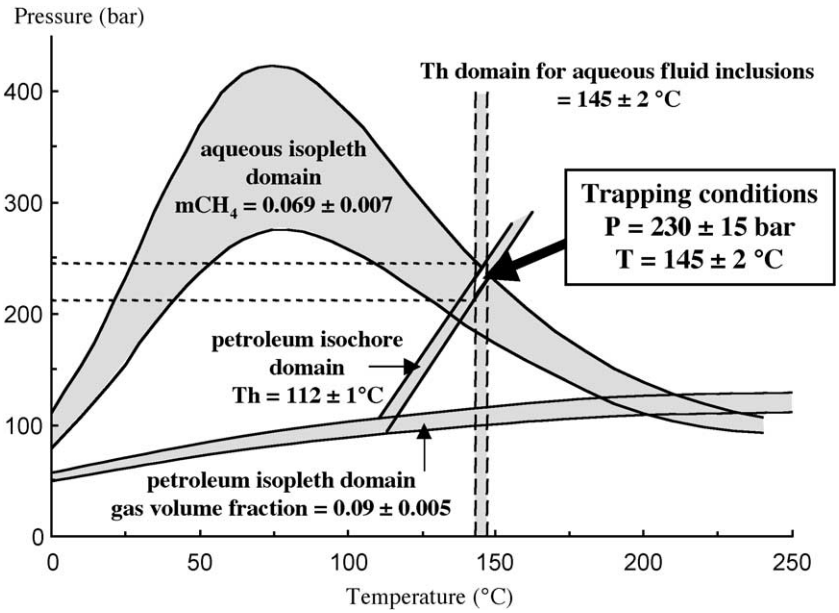

Fig. 8. $P-T$ diagram showing isopleths and isochores plotted from data obtained on petroleum and aqueous inclusions from the Cave-in-Rock fluorite deposit (Illinois).

0.069 ± 0.007 m. This value is in good accordance with the concentration of methane in the aqueous fluid inclusion determined by Raman analysis which is $mCH_4 = 0.071 \pm 0.007$ m. The Raman analysis of CH_4 in water–salt inclusions is consistent with the coexistence of aqueous and hydrocarbon fluids during the trapping of inclusions in the Cave-in-Rock sample.

4. Conclusions

The analysis of methane in NaCl bearing aqueous-rich fluid inclusions by Raman spectroscopy was calibrated using synthetic fluid inclusions in fluorite and quartz crystals between 100 and 200 °C and for NaCl concentration from 0 to 3.5 m. The inclusions were obtained between 150 and 250 °C in the liquid aqueous solution coexisting with a methane-bearing vapour phase in a gas-pressure autoclave. The concentration of methane in the aqueous solution was calculated using a computer programme (developed in Dubessy et al., 2001) incorporating the model of Duan et al. (1992). The Raman data obtained below and just above the homogenisation temperature were regressed as a function of temperature and NaCl concentration. This calibration allows the determination of the homogenisation pressure of methane bearing aqueous fluid inclusions provided their salinity and homogenisation temperatures are known. If aqueous fluid inclusions are coexisting with petroleum fluid inclusions, the $P-T$ conditions of hydrocarbon migration can be accurately determined.

Further work is necessary to evaluate the effect of temperature on the intensity of the water band for different salinities. The effect of different salts (NaCl, $CaCl_2$,...) having different interactions with water molecules should be explored for the analysis of methane concentration in salt bearing aqueous solutions. Finally, the effect of other gases, potentially present in petroleum environments (CO_2, H_2S, N_2) could be checked and their concentration measurement could be calibrated in the same way.

Acknowledgements

The authors greatly acknowledge A.M. van den Kerkhof and R.C. Burruss for their constructive reviews of this paper, and F. Noronha as associated editor. **[RR]**

References

Duan, Z., Moller, N., Greenberg, J., Weare, J.H., 1992. The prediction of methane solubility in natural waters to high ionic strength from 0 to 250 °C and from 0 to 1600 bars. Geochim. Cosmochim. Acta 56, 1451–1460.

Dubessy, J., Guillaume, D., Buschaert, S., Fabre, C., Pironon, J., 2000. Production of synthetic fluid inclusions using laser ablation in fluorite and quartz. An application to the H_2O-CH_4-NaCl system. Eur. J. Mineral. 12, 1083–1091.

Dubessy, J., Buschaert, S., Lamb, W., Pironon, J., Thiéry, R., 2001. Methane-bearing aqueous fluid inclusions: Raman analysis, thermodynamic modelling and application to petroleum basins. Chem. Geol. 173, 193–205.

Dubessy, J., L'Homme, T., Boiron, M.C., Rull, F., 2002. Determination of chlorinity in aqueous fluids using Raman spectroscopy of the stretching band of water at room temperature: application to fluid inclusions. Appl. Spectrosc. 56, 99–106.

Guillaume, D., Tkachenko, S., Dubessy, J., Pironon, J., 2001. High temperature and high pressure water solubility in ethylbenzene to 200 °C and 1 kbar and the acetic acid effect. Geochim. Cosmochim. Acta 65, 3319–3324.

Heidman, J.L., Tsonopoulos, C., Brady, C.J., Wilson, G.M., 1985. High-temperature mutual solubilities of hydrocarbons and water. AIChE J. 31, 376–384.

Pironon, J., Canals, M., Dubessy, J., Walgenwitz, F., Laplace-Builhe, C., 1998. Volumetric reconstruction of individual oil inclusion by confocal scanning laser microscopy. Eur. J. Mineral. 10, 1143–1150.

Pironon, J., Thiéry, R., Teinturier, S., Walgenwitz, F., 2000. Water in petroleum inclusions. Evidence from Raman and FT-IR measurements, PVT consequences. J. Geochem. Explor. 69–70, 663–668.

Poty, B., Leroy, J., Jachimowicz, L., 1976. Un nouvel appareil pour la mesure des températures sous le microscope: l'installation de microthermométrie Chaix-Méca. Bull. Soc. Fr. Minéral. Cristallogr. 99, 182–186.

Price, L.C., 1981. Aqueous solubility of crude oil to 400 °C and 2000 bar pressure in the presence of gas. J. Pet. Geol. 4, 195–223.

Ramboz, C., Pichavant, M., Weisbrod, A., 1982. Fluid immiscibility in natural processes: use and misuse of fluid inclusion data: II. Interpretation of fluid inclusion data in terms of immiscibility. Chem. Geol. 37, 39–48.

Richardson, C.K., Pinckney, D.M., 1984. The chemical and thermal evolution of the fluids in the Cave-in-Rock fluorspar district, Illinois; mineralogy, paragenesis, and fluid inclusions. Econ. Geol. 79, 1833–1856.

Roedder, E., 1984. Fluid inclusions. Reviews in Mineralogy, vol. 12. Mineralogical Society of America, Washington, DC, 644 pp.

Sawamura, S., Kitamura, K., Taniguchi, Y., 1989. Effect of pressure on the solubilities of benzene and alkylbenzenes in water. J. Phys. Chem. 93, 4931–4935.

Thiéry, R., Pironon, J., Walgenwitz, F., Montel, F., 2000. PIT (Petroleum Inclusion Thermodynamic): a new modelling tool for the characterisation of hydrocarbon fluid inclusions from volumetric and microthermometric measurements. J. Geochem. Explor. 69–70, 701–704.

Tsonopoulos, C., Wilson, G.M., 1983. High-temperature mutual solubilities of hydrocarbons and water: Part I. Benzene, cyclohexane and n-hexane. AIChE J. 29, 990–999.